Joule

CellPress

Article

Interactions between Lithium Growths and Nanoporous Ceramic Separators

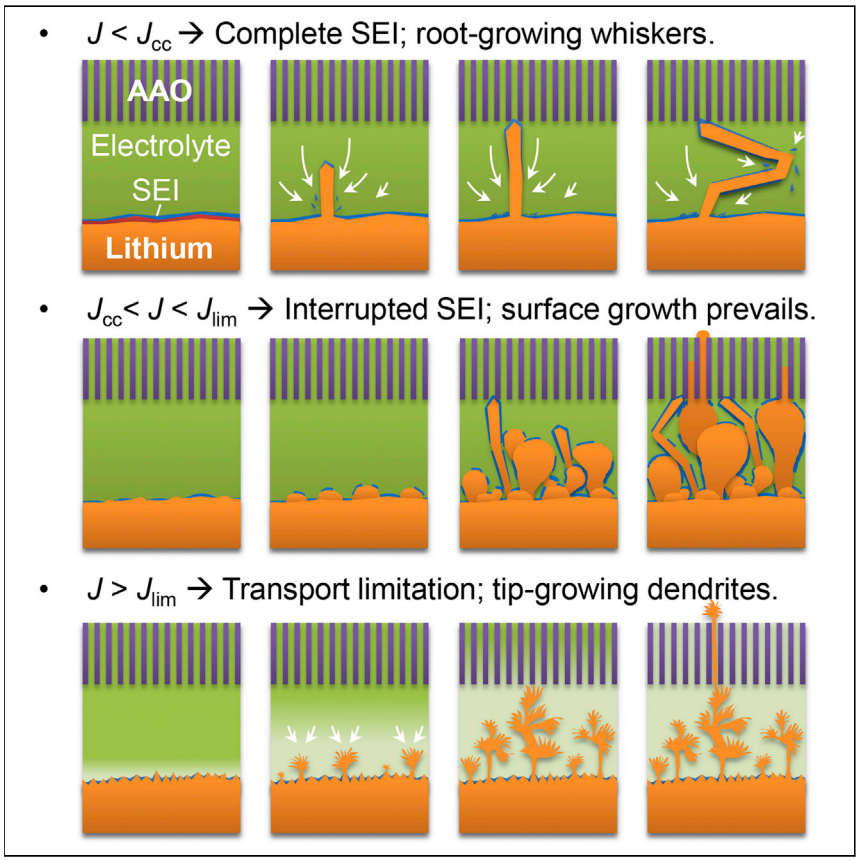

Depending on the operating current density, lithium electrodeposition exhibits three distinct growth modes: root-growing whiskers, surface-growing clusters, and tip-growing dendrites. While dendrites are the most penetrative deposit, they do not occur in practical batteries during normal operation, and the root-growing whiskers and surface-growing clusters fortunately can be blocked by ceramic separators. The detailed mechanisms revealed by this study provide guidelines to increase the safety of rechargeable lithium metal batteries.

Peng Bai, Jinzhao Guo, Miao Wang, ..., Ju Li, Fikile R. Brushett, Martin Z. Bazant

pbai@wustl.edu (P.B.)
bazant@mit.edu (M.Z.B.)

HIGHLIGHTS

Three current-dependent growth modes during Li electrodeposition are identified

Nanoporous ceramic separators can block Li growths up to a critical current density

Internal shorts at under-limiting currents are due to reaction-limited surface growth

Sudden voltage drops are signs of the metal penetration through the separator

Bai et al., Joule 2, 2434–2449
November 21, 2018
https://doi.org/10.1016/j.joule.2018.08.018

Joule

CellPress

Article

Interactions between Lithium Growths and Nanoporous Ceramic Separators

Peng Bai,[1,2,*] Jinzhao Guo,[1,3] Miao Wang,[2] Akihiro Kushima,[4] Liang Su,[2] Ju Li,[4,5] Fikile R. Brushett,[2] and Martin Z. Bazant[2,6,7,*]

SUMMARY

To enable lithium (Li) metal anodes with high areal capacity that can match advanced cathodes, we investigate the growth mechanisms and the tendency of the deposited metal to penetrate nanoporous ceramic separators across a range of practical current densities. Our results from realistic sandwich cells and special transparent junction cells suggest the existence of three growth modes of lithium, due to the competing reactions of lithium deposition and the solid electrolyte interphase formation. A critical current density (6 mA cm^{-2}), ~30% of the system-specific limiting current density, is identified as a practical safety boundary for battery design and operation, under which root-growing lithium whiskers are the dominant structure of electrodeposition and can be blocked by the nanoporous ceramic separator. Our operando experiments reveal that metal penetration of the separator does not lead to zero voltage immediately, but rather to sudden, small voltage drops, which should not be treated as benign soft shorts.

INTRODUCTION

Developing a stable rechargeable lithium (Li) metal anode has become an urgent need for the realization of post-Li-ion batteries, including Li-O_2, Li-S, and hybrid Li-flow batteries.[1–4] It also holds the promise to significantly increase the energy density of current Li-ion batteries by replacing the bulky graphite anode.[5] However, two major issues hinder the practical application of lithium metal anodes in rechargeable batteries. One is the internal short-circuiting of the cell by lithium metal whiskers and dendrites that can lead to catastrophic accidents. The other is the low Coulombic efficiency and therefore the short cycle life, caused by the continual consumption of active lithium and electrolyte components to form inert solid electrolyte interphase (SEI) layers on the surface of the non-uniform lithium deposits, during battery recharge. While the low Coulombic efficiency might be compensated by adding excess lithium or limiting the depth of charge/discharge, the risk of internal shorts is a serious drawback that must be solved to enable safe long-lasting rechargeable lithium metal batteries.

Among the latest studies on the mechanisms of lithium dendrite penetration, Lv et al.[6] reported that dendrite-induced short-circuiting was actually not found in coin cells using the common polyolefin separator (pore size 100–200 nm). Cell failure is more often attributed to electrolyte dry out due to continual SEI generation on the porous high-surface-area lithium deposits.[7,8] Indeed, the standard practice of using a lithium metal anode to evaluate the cycle life of a cathode material has never suffered from internal shorts. Such successes may have been enabled by the fact that the areal capacity of the lab-made cathodes are relatively low, so that only a small

Context & Scale

Li-ion batteries are energy-dense power sources of cell phones, laptops, and electric vehicles. The basic unit inside is a three-layer stack, i.e., anode, separator, and cathode, fully wetted by organic liquid electrolyte. Removing the ion-insertion anode materials could significantly increase the energy density of the battery. During recharge, Li ions that used to be accommodated by the anode materials will be reduced to form a Li metal anode, without dead weight and volume. The process, however, is notoriously unstable and always forms finger-like structures that can penetrate the separator to short-circuit the battery, through mechanisms more complex than the simple term "dendrite" can reveal. Depending on the current, one may generate tip-growing dendrites, root-growing whiskers, or surface-growing clusters. This study presents the accurate understanding of each growth mode, which is critical for controlling the hazardous instabilities across the entire range of working conditions.

amount of lithium (~1 mAh cm^{-2}) is being deposited and dissolved in each cycle. However, when more practical cathode loadings are used, where the areal capacities are larger than 2 mAh cm^{-2}, the behavior of lithium metal anodes becomes drastically different,[9] and lithium penetration through nanoporous separators can easily occur.[6,9] It is critical to understand and predict the precise conditions for such short circuits, before one can optimize the design and operation of rechargeable metal batteries.

A quantitative safety boundary, called Sand's capacity, was recently proposed based on experiments in special capillary cells.[10] This characteristic capacity marks the transition between two distinct growth mechanisms of lithium metal in liquid electrolytes: (1) at current densities greater than the intrinsic diffusion-limited current density (over-limiting current density), once the charged capacity exceeds Sand's capacity, lithium grows at the outermost tips of the electrode surface to form fractal "dendritic" structures; (2) at current densities lesser than the diffusion-limited current density (under-limiting current density), or before the Sand's capacity, lithium primarily grows from the root, like human hairs, to form "mossy" structures.[10] Because the deposits formed prior to Sand's capacity can be blocked by a nanoporous ceramic separator, whereas deposits formed afterward cannot, Sand's capacity can be considered as a safety boundary to avoid the tip-growing dendrites. However, due to the small inter-electrode separation in practical batteries, Sand's capacity appears too high to be useful. Moreover, for under-limiting, but still relatively large, current densities, lithium penetration can still occur. For this regime of reaction-limited lithium growth, more accurate critical safety boundaries must be identified.

In the present study, we constructed two types of symmetrical lithium cells to investigate the safety boundaries in terms of the applied current density and areal capacity beyond which nanoporous ceramic separators can no longer block the metal growth and internal shorts become inevitable. The first set of experiments exploits a sandwich structure, which consists of lithium electrodes, an anodic aluminum oxide (AAO) separator, and polyvinylidene fluoride (PVDF) washers on both sides of the AAO to create two electrolyte-filled compartments. The second set of experiments uses a junction cell consisting of two segments of straight glass capillary and a small piece of AAO separator, all sealed in transparent epoxy resin.

Using both types of experiments, we identify two critical current densities that separate three different growth modes of greatly varying safety risk. Below the first critical current density, J_{cc}, lithium grows primarily from the root to form whiskers, which may be attributable to the complete coverage of the lithium surface by a robust SEI layer. Beyond the second critical current density, J_{lim}, the system-specific diffusion-limited current density, ion depletion at the electrode surface leads to the diffusion-limited, tip-growing, dendritic lithium that can easily penetrate the AAO nanopores and short the cell. Between these two critical current densities, the SEI formation could be interrupted by the competing lithium deposition, leaving parts of the metal surface without the continuous SEI coverage, such that near isotropic surface growths start to prevail. Based on these findings, we propose a set of safety boundaries along with strategies to optimize the design of rechargeable metal batteries.

RESULTS

Figure 1 displays the structure of the sandwich cell and the transient voltage responses to galvanostatic electrodeposition at 1 mA cm^{-2}. At first glance, the steep

[1]Department of Energy, Environmental and Chemical Engineering, Washington University in St. Louis, One Brookings Drive, Saint Louis, MO 63130, USA

[2]Department of Chemical Engineering, Massachusetts Institute of Technology, 77 Massachusetts Avenue, Cambridge, MA 02139, USA

[3]Department of Mechanical Engineering and Materials Science, Washington University in St. Louis, One Brookings Drive, Saint Louis, MO 63130, USA

[4]Department of Nuclear Science and Engineering, Massachusetts Institute of Technology, 77 Massachusetts Avenue, Cambridge, MA 02139, USA

[5]Department of Materials Science and Engineering, Massachusetts Institute of Technology, 77 Massachusetts Avenue, Cambridge, MA 02139, USA

[6]Department of Mathematics, Massachusetts Institute of Technology, 77 Massachusetts Avenue, Cambridge, MA 02139, USA

[7]Lead Contact

*Correspondence: pbai@wustl.edu (P.B.), bazant@mit.edu (M.Z.B.)

https://doi.org/10.1016/j.joule.2018.08.018

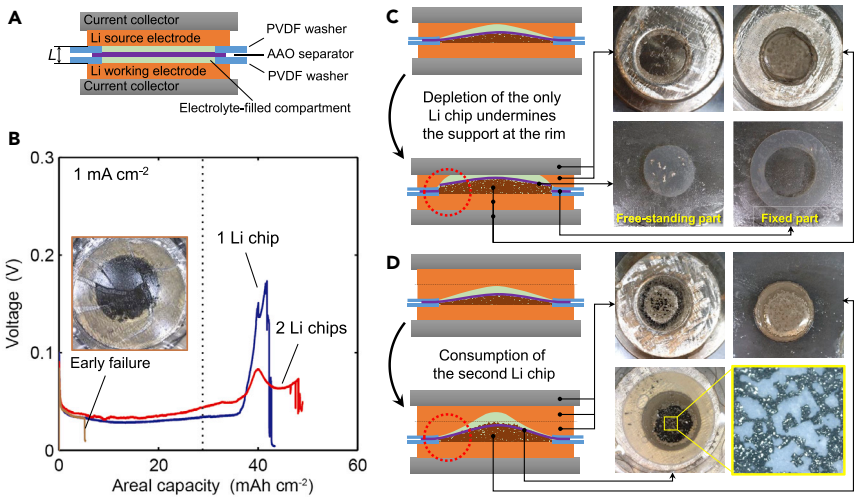

Figure 1. Postmortem Analyses of the Galvanostatic Lithium Electrodeposition at 1 mA cm^{-2}

(A) Schematic structure of the sandwich cell.

(B–D) Voltage responses of the galvanostatic electrodeposition process. The black dotted line indicates the theoretical areal capacity that can be deposited into the electrolyte-filled compartment between Li working electrode and the AAO of the sandwich cell. The inset displays the photograph of a randomly ruptured AAO separator due to improper assembly, which led to the early failure (B). Photographs and schematic explanation of (C) the shorted cell with only one lithium chip that exhibited a very steep voltage spike, and (D) the shorted cell with two lithium chips that exhibited instead a small voltage hump. The red dotted circles highlight the differences in Li dissolution at the source electrodes.

voltage increase observed in Figure 1B appears similar to Sand's behavior due to ion depletion near the electrode surface, which creates a non-conductive region and necessitates an increased polarization to maintain constant current density.[10] However, this current density (1 mA cm^{-2}) is well below the estimated diffusion-limited current density (20 mA cm^{-2}), according to the dilute solution theory[10] $J_{lim} = 2z_c c_0 F D_{app}(t_a L)^{-1}$. Here, $z_c = 1$ is the charge number of the lithium cation, $c_0 = 1$ M is the bulk electrolyte concentration, F is the Faraday constant, $D_{app} = 2 \times 10^{-6}$ cm^2 s^{-1} is an averaged apparent diffusion coefficient of lithium cations in 1 M liquid electrolyte,[10] $t_a = 0.62$ is the transference number of the hexafluorophosphate anion (PF_6^-), and $L = 300$ μm is the inter-electrode distance in the sandwich cell. Therefore, the voltage spikes must come from other processes. Upon disassembling the cell post test, the lithium source electrode was almost completely consumed, and the bare surface of the stainless steel current collector was clearly visible (Figure 1C). This implies that the voltage spike was the result of the depletion of the lithium source electrode, instead of ion depletion in the electrolyte.

We then doubled the amount of lithium source by using two lithium chips as the source electrode (Figure 1D). The voltage spike disappears, but is replaced by a small hump (red curve in Figure 1B), which can be attributed to the dissolution of the second lithium chip. Postmortem analyses of the one-Li-chip (Figure 1C) and two-Li-chip (Figure 1D) experiments revealed that, in the former experiment, the free-standing part of the AAO was punched through such that the edges perfectly match the inner diameter of the PVDF washer, while, in the latter experiment, the AAO was only slightly distorted and remained intact. As schematically explained in Figure 1C, depletion of the single lithium chip significantly undermined the mechanical support to the AAO at the inner rim of the washer. In the control experiment with two lithium chips (Figure 1D), dissolution occurred preferentially at the center of

the second lithium chip, thus the support to AAO at the inner rim of the washer was less affected. In both cases, however, a large amount of lithium was successfully deposited inside the lower compartment *before* the fracture of or metal penetration into the AAO. This is consistent with the observed smooth voltage responses before the sudden voltage drop. The results suggest that lithium growths under very low current densities can be blocked by the nanoporous ceramic separator.

Further experimental results from galvanostatic electrodeposition at 1 mA cm^{-2} and higher current densities are displayed in Figure 2. The experiments were repeated five times at each current density to determine an average response and measurement uncertainty introduced during the cell assembly. As the current density increases, the sudden voltage drop occurs sooner. We took the areal capacities at the first sudden voltage drop to be the penetration capacities (solid arrow head in Figures 2A–2E) and plotted them against their corresponding current densities in Figure 2F, where the dotted line is the theoretical areal capacity (thickness) of lithium metal that can be accommodated in the lower compartment of the sandwich cell. Figure 2F clearly shows that the lithium deposits tend to completely fill the compartment before they penetrate AAO at current densities below 6 mA cm^{-2}. For higher current densities approaching the limiting value (20 mA cm^{-2}), lithium deposits become increasingly penetrative, leaving the lower compartment less filled (Figure 2F).

To further verify the above interpretation, we applied an over-limiting current density of 50 mA cm^{-2} to the sandwich cells to make the effects of lithium penetration more pronounced and easier to identify. During the deposition, three features were identified in the voltage responses (Figure 3): (1) a voltage increase due to strong concentration polarization (i.e., Sand's behavior[10]), (2) a linear slope, and (3) a sudden drop with a noisy tail.

The linear slope could be attributed to the process of dendrite penetration, as will be discussed later in the transparent junction cell. Comparing the magnitude of the voltage and the time (capacity) accumulated awaiting the penetration, it is clear that the AAO separator with smaller pore size exhibited much higher resistance to penetration than that with larger pores. Figure 3B is an optical micrograph of the Li-penetrated AAO harvested from the short-circuited cell, on which a dark region is visible on the upper side (facing the source electrode). We broke the AAO across this region and investigated the morphologies by scanning electron microscopy (SEM). Indeed, very thin lithium filaments were found there, which were responsible for the sudden voltage drop. A large amount of porous lithium deposits was found beneath the AAO, i.e., in the lower compartment (Figure 1A).

To correlate electrochemical responses with physical processes more clearly, we devised a transparent miniature cell with glass capillaries to visualize the operando penetration process. As seen in Figure 4B, similar features emerged in the voltage response when the same over-limiting current density of 50 mA cm^{-2} was employed: (1) strong polarization due to Sand's behavior, (2) a linear voltage slope, and (3) a sudden voltage drop and decay. From time point C to point F (labeled in Figure 4B), the electrode on the right was pushed backward for 11 μm, while the dendritic lithium deposits were advancing through the nanochannels of the AAO. The capacity delivered by point F was 0.97 μAh, which is equivalent to a 6.8-μm-thick disk of lithium metal within the capillary (300 μm diameter). Neglecting the volume of lithium in the AAO channels and the volume of the SEI layers covering the deposits,

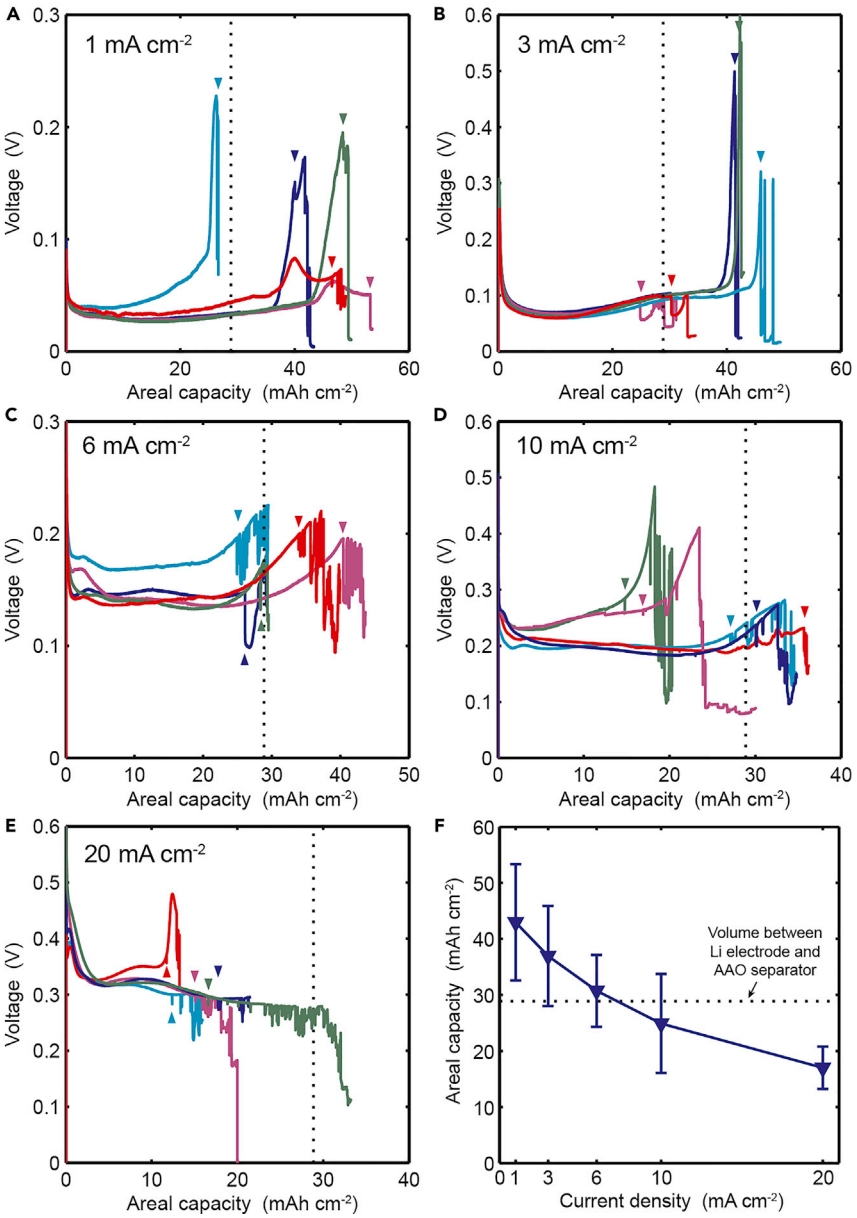

Figure 2. Galvanostatic Lithium Electrodeposition at Various Current Densities

(A–E) Voltage responses at (A) 1 mA cm^{-2}, (B) 3 mA cm^{-2}, (C) 6 mA cm^{-2}, (D) 10 mA cm^{-2}, and (E) 20 mA cm^{-2}. Each experiment was repeated five times as indicated by different colors. Black dotted lines indicate the theoretical areal capacity that can be deposited into the electrolyte-filled compartment between Li electrode and AAO of the sandwich cell.

(F) Current-dependent penetration capacities defined and sampled at the first sudden voltage drops indicated by the solid arrow heads. Error bars indicate the standard deviation of each dataset.

we estimated the porosity of the deposited lithium in our miniature cell to be 38% based on the difference in the theoretical (6.8 μm) and experimental (11 μm) lengths.

Our operando experiment raises a question of how to judge an internal short by simple inspection of the electrochemical responses. As is evident in Figure 4B, lithium penetration into the AAO at point F did not lead to zero voltage. Even after physical

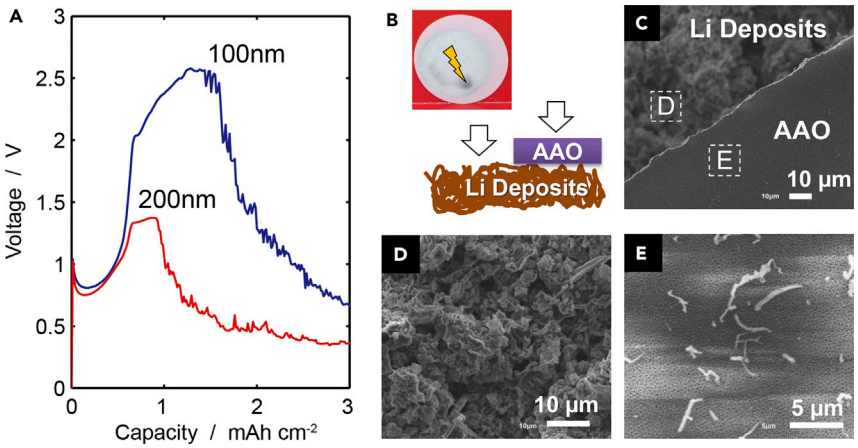

Figure 3. Lithium Penetration at an Over-Limiting Current Density of 50 mA cm^{-2}

(A) Voltage responses of sandwich cells using AAO separators of two different pore sizes.

(B–E) Photograph of the AAO harvested from the short-circuited cell. The AAO was broken around the dark region to prepare a Li/AAO composite sample as depicted by the cartoon (B). Scanning electron microscopy (SEM) images of (C) the Li/AAO composite, (D) the porous lithium deposits beneath the AAO, and (E) the thin filaments of lithium metal on top of the AAO.

contact is made between the lithium deposits and the source electrode (time points G through H in Figure 4B), the magnitude of the voltage appears comparable with the initial voltage in the experiment (time point C). This phenomenon is likely due to the insulating properties of the SEI layers coating the lithium deposits. Thus, such "soft shorts," defined as the sudden small drops in the voltage response, require special attention.[5] Since the time interval from point C to point D in Figure 4B is only 2 min, the voltage variation in between will appear like a negligible voltage spike in a long-duration cycling profile. According to our results, a sudden voltage drop (time point F in Figure 4B), is indicative of lithium penetration through the separator, even though the penetrated deposits (circled part in Figure 4F) may not have touched the source electrode and the voltage appeared "normal." This is why we defined the first sudden voltage drops in Figure 1 as the sign of the dendrite penetration, regardless of the magnitude of the voltage drop and the absolute values of the resultant voltage.

Growth Modes

By designing unique experimental cells and combining operando experiments with postmortem analyses, we clarified the details of lithium growth mechanisms in liquid electrolyte. As summarized schematically in Figure 5, lithium grows in different modes and into different morphologies/microstructures depending on the applied current densities. When a low current density is applied (<6 mA cm^{-2}, or 30% of the limiting current density, for the sandwich cell in this work), the electrochemical reduction of electrolyte components leads to the formation of a complete coverage of robust SEI on the surface of the lithium metal anode at an early stage. Li cations can steadily diffuse across and deposit beneath the SEI layers, causing an increase in internal pressure.[11] At a certain point, when the pressure reaches a threshold, it will squeeze a plastic flow of lithium metal out of the SEI coat through a pinhole (Figure 5B). With very little coverage on the side walls of the protruding whisker, especially at the newly exposed part (Figure 5C), i.e., the root, further deposition leads to the root-growing phenomenon. Because the tip of whisker is being pushed from behind, penetrating through the channels of AAO is akin to threading a needle

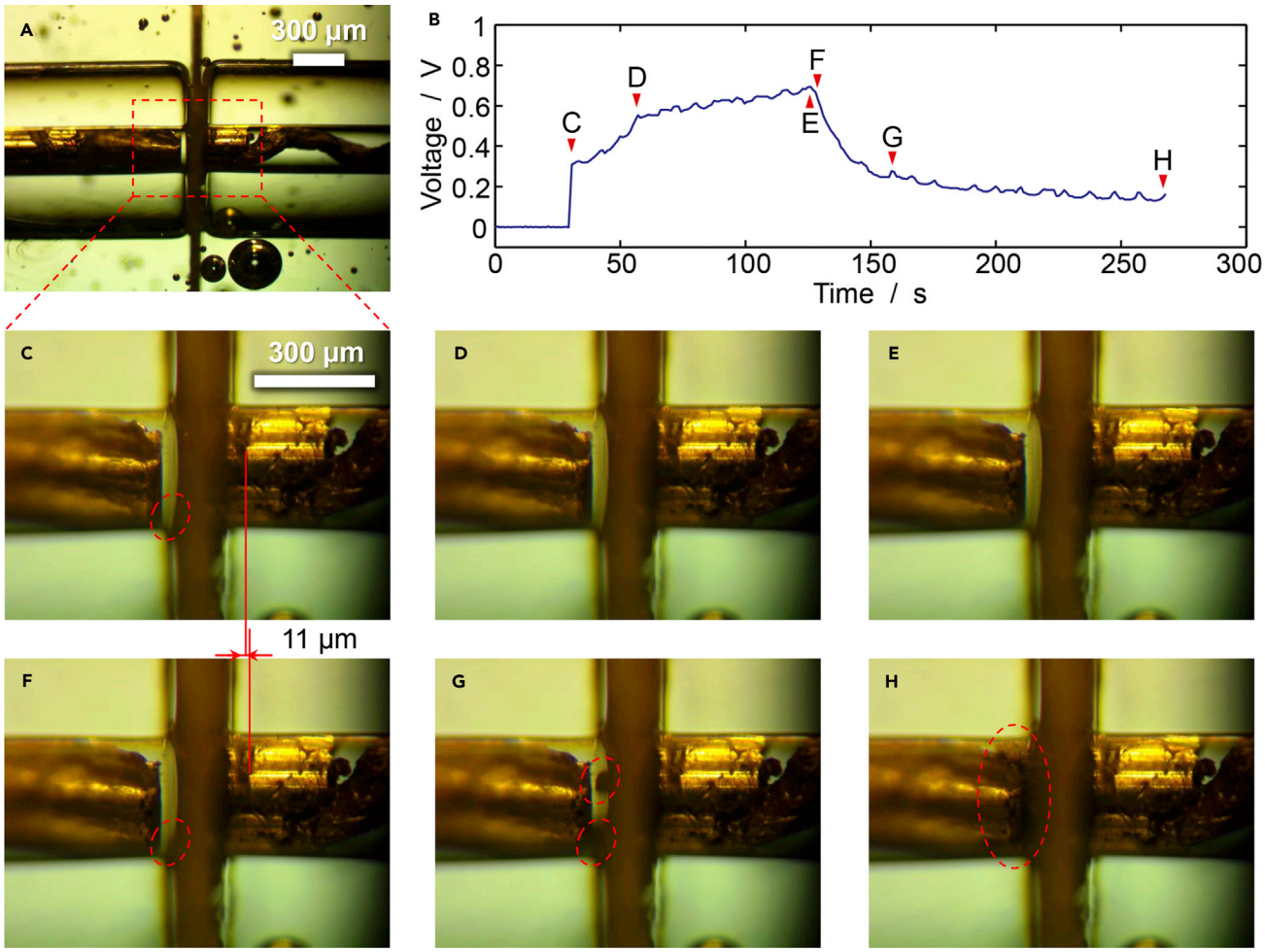

Figure 4. Operando Investigation of Lithium Penetration at High Current Densities

(A) The junction cell made of two segments of glass capillaries and a small piece of AAO, which are all sealed in epoxy. During experiment, Li cations dissolve from the source electrode on the left and move across the separator to deposit onto the Li electrode on the right. Distance between two Li electrodes is around 260 μm, similar to that of the sandwich cell.

(B) Voltage responses of the junction cell during electrodeposition at the same over-limiting current density of 50 mA cm^{-2} as used in the sandwich cell experiment.

(C–H) Corresponding snapshots during the course of experiment. No significant changes can be identified in (D) and (E) awaiting the metal penetratoin through AAO. Comparison of the circled parts in (C) and (F) reveal protrusion of lithium deposits in the left compartment. Circled parts in (G) and (H) highlight the additional Li penetration through AAO.

and is actually even more difficult as the whiskers are usually wider than the nanochannels, especially in ether-based electrolytes.[12–14] Instead, the growing lithium whiskers are forced to kink, elongate, and spread below the AAO, until the mechanical pressure applied by the growing deposits is sufficient to punch through the separator (Figure 1C).

At the other limit, when over-limiting current densities are applied (>20 mA cm^{-2} for the sandwich cell in this work), instability will occur at Sand's time. Tip-growing dendritic lithium then explosively grows out to catch up the retreating concentration front in the electrolyte in order to maintain the required constant current density.[10] In this case, penetrating through the nanochannels becomes much easier and only takes a few minutes (Figures 3 and 4).

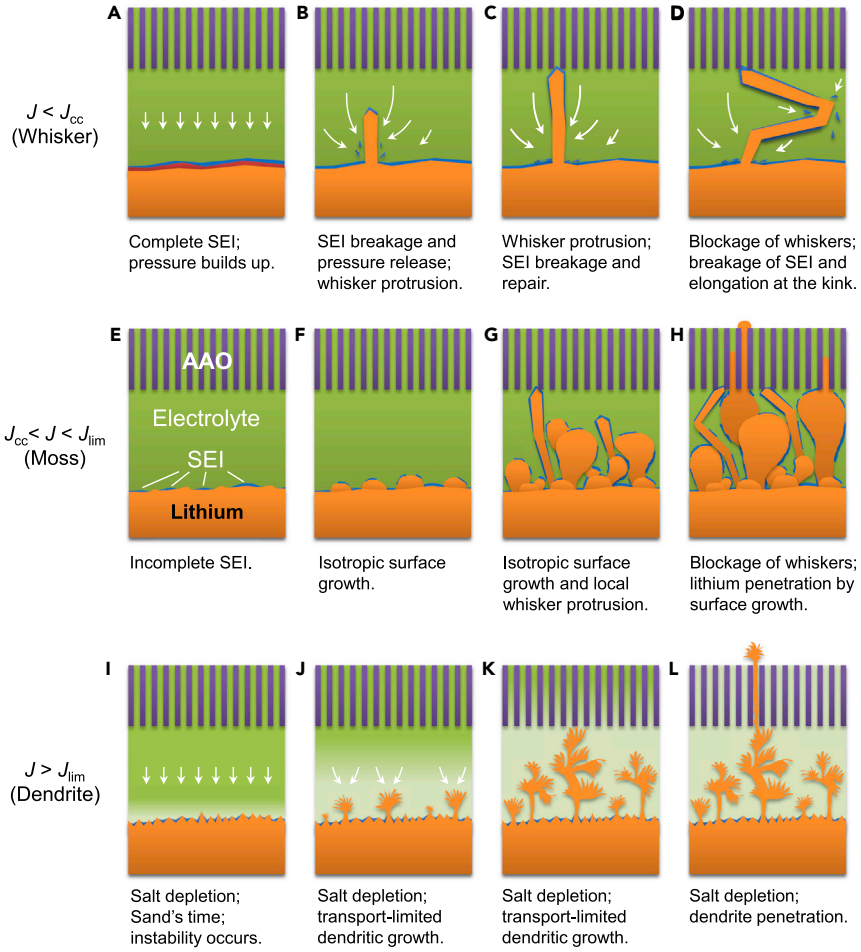

Figure 5. Schematic Summary of the Lithium Growth Mechanisms and Interactions with the Nanoporous Ceramic Separator

(A–D) Schematic explanation of whisker protrusion from the root, when the applied current densities are lower than the critical current density, J_{cc}.

(E–H) Schematic explanation of the emergence of surface growths due to the imcomplete SEI layers interrupted by the increased current density.

(I–L) Schematic explanation of the transport-limited, tip-growing, dendritic lithium, triggered by over-limiting current densities.

Arrows indicate the directions of ionic flux.

The most interesting scenario, however, occurs when an intermediate current density is applied, under which the rate of lithium deposition becomes comparable with the rate of SEI formation. At such rates, $J_{cc} < J < J_{lim}$, complete coverage of robust SEI may easily be interrupted by lithium deposits (Figure 5E) that quickly form at the most favorable locations on the electrode surface. In such areas without complete SEI coverage, further deposition of lithium cations favors more isotropic surface growths. In other areas, however, the robust SEI can still trigger the growth of lithium whiskers via the mechanism described earlier. The interplay between these growth modes leads to a mossy structure. While the whiskers may still be blocked, the surface growth can penetrate the ceramic nanopores. As the current density increases, more surface growths will be favored, which promotes the metal penetration through the separator (Figure 2F).

We propose that this new transition in reaction-limited surface growth reflects the different overpotential dependencies of the competing deposition and passivation reactions[15–17]: (1) electrodeposition of lithium cations to form metallic lithium (R_{Li}); (2) reaction of anions to form the inorganic components of the SEI (R_{inSEI}); and (3) reaction of solvents to form the organic components of the SEI (R_{orSEI}). The first two reactions are sensitive to the local overpotential, as well as the depletion of salt concentration at higher current densities. The third reaction proceeds even in the absence of applied current and is able to passivate the electrode surface in less than 1 s,[18] apparently with negligible overpotential dependence (despite the possibility of coupled electron transfer reactions in corrosion processes). As the applied current density increases, the associated higher overpotentials significantly promote electrodeposition (R_{Li}). At the same time, inorganic SEI growth (R_{inSEI}) is diminished by the progressive depletion of anions from the electrode surface, as well as electron transport limitations across the SEI layer, while organic SEI growth (R_{orSEI}) is largely unaffected by the overpotential and proceeds slowly due to the sluggish electron transport across existing SEI. The net result is an interrupted heterogeneous SEI coverage, leading to mossy surface growth. Moreover, the competition of these reactions is sensitive to the history and state of the electrode surface. For example, lithium electrodeposition on gold electrodes in DMSO electrolyte exhibits whisker growth at high overpotentials and cauliflower-like structures at low overpotentials,[19] while solvent-diffusion-limited SEI growth on graphite insertion electrodes can explain the long-term degradation of lithium ion batteries under various cycling protocols.[20] Here, we identify, for the first time, the macroscopic consequences of these new growth modes of lithium deposits on lithium electrodes for metal/separator interactions and battery safety.

Safety Boundaries

The mechanisms above indicate three safety boundaries that can be quantitatively defined and exploited to increase the safety of rechargeable metal batteries. (1) The critical current density J_{cc} (~30% J_{lim}), below which the thick root-growing lithium whiskers can be easily blocked by available nanoporous ceramic[10] or polyolefin[6] separators, should be experimentally identified for practical cells. (2) The electrolyte composition and separator pore sizes should be optimized synergistically, so that surface growths at higher current densities can be restrained by counteracting the SEI-modified surface energy of the lithium deposits. (3) While the practical current densities in fresh commercial cells using liquid electrolytes are well below their intrinsic limiting current densities, monitoring the deterioration of the ion transport kinetics to alert the value of the real-time limiting current density is key to avoid tip-growing lithium dendrites.

DISCUSSION

Lithium Growth Dynamics

While the root-growing whiskers cannot be predicted by existing mathematical models, surface-growing clusters may, in principle, be simulated by a thermodynamically consistent electrochemical phase field model. Recently, García and coworkers[21,22] applied the classical phase field method to model the electrodeposition of lithium and investigate the interaction between the growths and a rigid porous separator, dominated by surface tension (contact angle and curvature of a pure lithium surface entering the pores). In the notation of this theory, our experiments, showing that growth at 1 mA cm^{-2} can be readily blocked by rigid nanopores of 100–200 nm in diameter correspond to a dimensionless current density of 50 and a dimensionless pore size range of 0.08–0.16,[22] which sits in a theoretically predicted "short-circuit regime" (Figure 6 in Jana et al.[22]), despite the fact that

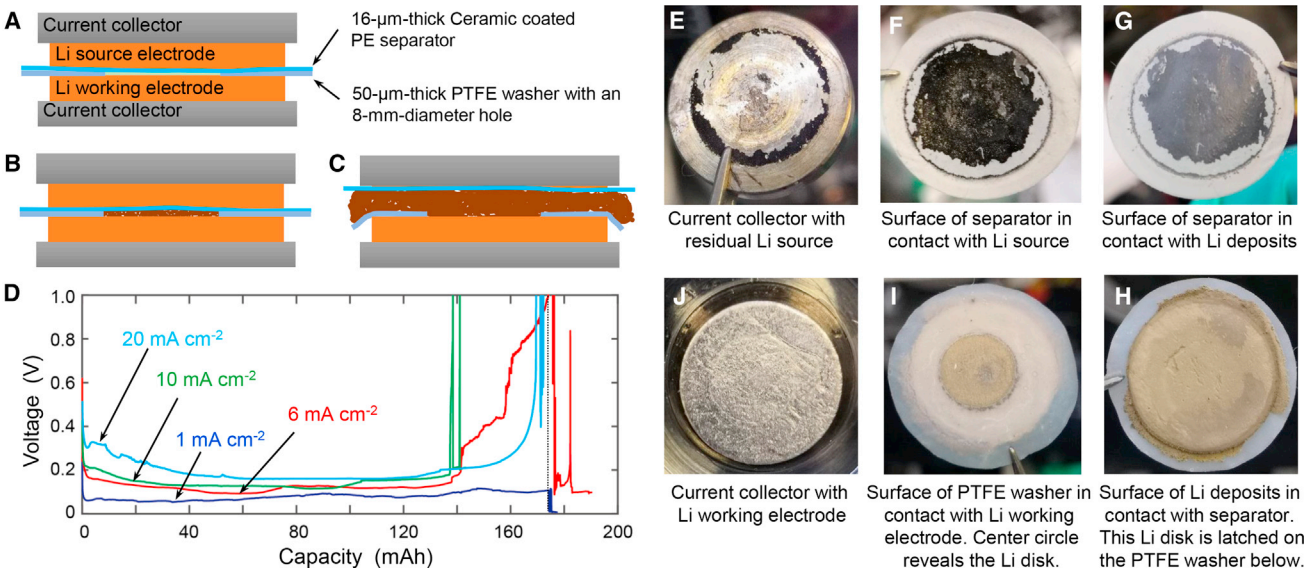

Figure 6. Postmortem Analyses of the Galvanostatic Lithium Electrodeposition Using Commercial Ceramic-Coated Separator

(A) Schematic structure of the sandwich cell.

(B) Schematic explanation of the initial stage of electrodeposition, where the deposits filled the shallow compartment formed by the PTFE washer.

(C) Schematic explanation of the final stage of electrodeposition, where the deposits grew laterally and the ceramic separator was pushed up toward the current collector without metal penetration.

(D) Voltage responses of the galvanostatic electrodeposition process at various nominal current densities. The black dotted line indicates the theoretical areal capacity of the 450-μm-thick lithium source electrode.

(E–J) Digital photographs of the components of sandwich cell post test. (E) The stainless steel current collector with residual lithium source electrode. The ceramic-coated separator (F) with residual lithium source electrode on one side and (G) without visible damage on the other side. (H) The top surface of the disk of lithium deposits in contact with the separator. (I) The bottom surface of the disk of lithium deposits latched on the PTFE washer. (J) The lithium working electrode.

short-circuiting was never observed. This discrepancy between theory and experiment, however, is not surprising, since the simulations assume a pure lithium solid (as defined by the order parameter and illustrated by the solid orange color) and a single electrodeposition reaction, while, in reality, the deposits are highly porous and chemically heterogeneous, composed of lithium whiskers and clusters that form a porous lithium/SEI composite, as a result of competing passivation and deposition reactions. To better capture the interactions between the metal growths and the ceramic separator, it may be helpful to assume a homogenized porous medium, whose chemical, physical, and mechanical properties could, in principle, be revealed by systematic comparison of simulations and experiments including both imaging and electrochemical data.

The discrepancy between our experiments and existing simulations is also exacerbated by the inaccuracy of the two key parameters adopted in mathematical models. The first is the SEI conductivity, which depends on the composition and microstructure of the heterogeneous interphase region and is known to be sensitive to the local constituents of the electrolyte.[23] The second is the lithium metal surface energy, which, unfortunately, is complicated by the competing growth of SEI layers and clearly heterogeneous. As also suggested by Wu et al.[24], the key to unifying the mechanisms within a single theoretical framework is to accurately capture the interplay between lithium metal growths and the SEI evolution. If the conductivity of the SEI layers formed under various dynamic conditions and the surface energy of the SEI-modified lithium metal can be obtained, predictions of the critical size of separator pores versus current densities,[22] as well as the critical size of lithium nuclei

versus overpotential,[25] may become more accurate and powerful. Still, it is noteworthy that absolute magnitudes of the current densities from different reports are not meaningful for cross-system comparison. It is the relative current density, with respect to the system-specific limiting current density, that primarily determines the dynamics of the interphase and the morphology of lithium deposits.

Existing Ceramic Separators/Electrolytes

The findings presented here are consistent with the superior performance of composite ceramic separators/electrolytes reported by Archer's group.[26,27] With the polymer-AAO-polymer composite separators/electrolytes, the lithium metal cells demonstrated more than 1,000 hr of stable cycling, at current densities up to 1 mA cm^{-2}. Using the available parameters, a rough estimation of the limiting current for the system with an 800-μm-thick separator is 8 mA cm^{-2}. While our results suggest that a lithium metal cell may be able to survive higher current densities up to 30% of its limiting current ($J_{cc} \sim 30\%\ J_{lim}$), the precise J_{cc} and J_{lim} values for a specific system must be identified experimentally. For this polymer-AAO-polymer composite, the apparent diffusion coefficient could be much lower than the value we used for the free electrolyte, due to more sluggish transport through the polymer layers, which will further lower the limiting current density. On the other hand, the AAO membrane in the composite separator has a much smaller pore size of only 20 nm, which will make the penetration of surface growth much more difficult.

Layers of ceramic particles have been coated onto traditional polyolefin separators to keep the polymer sheet from shrinking under high temperature conditions. These types of separators are believed to be able to block lithium "dendrites," where the blocked deposits are actually whisker and surface growths, not the dendritic growth. As a direct extension of our findings, a commercial ceramic-coated polyethylene (PE) separator was used in lithium metal symmetric cells without the 127-μm-thick PVDF washers to investigate the metal penetration or blockage behaviors. As shown in Figure 6A, a 16-μm-thick separator was introduced between the lithium source electrode and the lithium working electrode. Between the separator and the working electrode, we used a much thinner (50 μm) polytetrafluoroethylene (PTFE) washer to define the active area on the working electrode, otherwise electrodeposition will occur on the inner surface of the stainless steel cell wherever in contact with the liquid electrolyte. To calculate the limiting current of this new configuration, we used the separator thickness, i.e., 16 μm, and tortuosity determined by phase contrast X-ray computed tomography,[28] i.e., $\tau = 3.43$, for the same separator from MTI. The formula[29] $D_{porous} = D_{app}/\tau$ is adopted to correct the averaged apparent diffusion coefficient for free electrolyte D_{app} and better represent the ion transport through porous media. The resulting limiting current density is 109 mA cm^{-2}. At practical current densities, and even the aggressive current densities used in this study ($\leq$20 mA cm^{-2}), dendritic growths will not be triggered.

As clearly seen in Figure 6D, and in stark contrast to Figure 2, no sudden voltage drops were observed during the constant current electrodeposition, until the (near) depletion of the lithium source electrode. Figures 6E–6J reveal that the lithium source electrode was almost entirely transferred to the other side the separator, as schematically illustrated by Figures 6B and 6C. Note that the current densities labeled in Figure 6D are valid only for the initial stage. Once the compartment of the PTFE washer is filled (Figure 6B), the deposits begin to grow laterally (Figure 6C), instead of perpendicularly to penetrate the very thin separator, as demonstrated by the lack of sudden voltage drops.

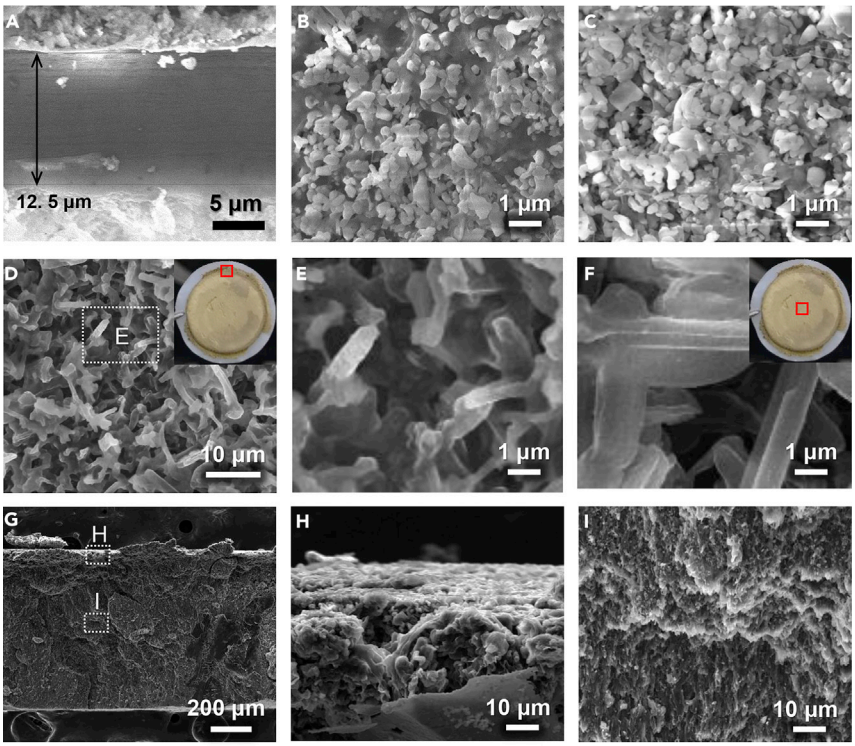

Figure 7. SEM Images of the Commercial Ceramic-Coated Polyethylene Separator and the Rigid Lithium Deposit Disk

(A–C) Cross-sectional (A), upper (B), and lower (C) surfaces of the ceramic-coated PE separator.

(D–F) Low- (D) and high-magnification (E and F) images of the surface of lithium deposit. The insets showed the locations on the deposit disk where the SEM images were taken.

(G–I) Low- (G) and high-magnification (H and I) images of the cross-section of the lithium deposit disk.

The capability of blocking the growths is attributable to the densely packed submicron-sized alumina (Al_2O_3) particles on the surface of the 12.5-μm-thick PE middle layer (Figure 7A). The fine and tortuous pores between the Al_2O_3 particles (Figures 7B and 7C) successfully blocked the wide lithium whiskers and plates (Figures 7E and 7F) from penetrating the separator. The thickness of the lithium deposit disk is measured to be 790 μm thick (Figure 7G). Compared with the thickness of the fresh lithium chip, the porosity of the lithium deposit disk is estimated to be 43%, which is very close to the porosity estimated from the junction cell experiments. This further justifies the need to take into account the porous nature of lithium deposits when investigating the growth dynamics and instabilities or evaluating the practical energy density of rechargeable metal electrodes.

The set of growth mechanisms identified here also has important implications for rechargeable metal batteries using solid electrolytes. While the significant portion of the work in the solid electrolyte field has focused on improving the ionic conductivity, making the electrolyte thin enough to avoid transport limitation is equally important,[5,30] especially given the evidence that 1-mm-thick high-conductivity (~0.5 mS cm^{-1}) solid electrolytes usually cannot sustain a current density higher than 0.5 mA cm^{-2} without lithium penetration.[31–34] This is consistent with an estimation made by Koch and coworkers that, for 1-mm-thick solid electrolytes or structured electrolytes, the limiting current density could be as low as 0.35 mA cm^{-2},[35,36] which indicates that the cells[31–34] were very likely working at

the over-limiting-current regime and the transport-limited tip-growing dendrites easily grew along the ionic pathway[10] inside the solid electrolytes to short the cells. Reducing the thickness of the solid electrolytes while increasing the conductivity may eventually increase the limiting current density, so that the operation at 0.5 mA cm^{-2} falls into the under-limiting-current regime, where the theoretical predictions from linear stability analyses pioneered by Monroe and Newman,[37] and recently extended by Srinivasan and coworkers[38,39] become applicable, before surface[40] or bulk[41] defects begin to undermine the robustness of the solid electrolytes.

Our present study focuses on the metal penetration mechanisms through special ceramic separators during one-way constant current electrodeposition. Future efforts should focus on cycling lithium metal anodes in cells containing high areal-capacity intercalation cathodes, and commercial separators. The types and amounts of liquid electrolytes used in the experimental cells should also be carefully controlled to investigate the probability of battery failures due to metal penetration as opposed to impedance rise.

Conclusions

We have investigated lithium electrodeposition using specialized experimental cells under various constant current densities. Combining the operando observations in the transparent junction cells with the postmortem analyses of the more realistic sandwich cells provides a reliable yet economical platform to assess the performance of novel electrolytes and electrode systems operating at higher areal capacities. Our work manifests the importance of correlating electrochemical responses to morphology changes.[42] Our results suggest that there exist (at least) three current-dependent growth modes. Below a critical current density, J_{cc}, at which the rate of lithium deposition is much slower than the rate of SEI formation, complete coverage of robust SEI can be achieved triggering root-growing lithium whiskers as a consequence of the release of internal pressure built under the SEI layer. In the intermediate regime, where the rate of lithium deposition and rate of SEI formation become comparable, complete coverage of robust SEI will be hindered by rapid growth of local lithium deposits. The competing whisker and surface growths will form a mossy structure, in which the surface growths can penetrate the nanoporous separators. Beyond the system-specific diffusion-limited current density, J_{lim}, tip-growing dendrites can easily penetrate the nanopores in the separator.

These findings have important implications for the design of rechargeable lithium metal batteries with three layers of safety boundaries: (1) identifying J_{cc} (~30% J_{lim}) for specific cells so that only the whiskers will be generated and safely blocked; (2) modifying the electrolyte and tuning the composition of SEI so that smaller stiff pores can overcome the surface energy of SEI-covered lithium metal and prevent penetration at higher current densities; and (3) monitoring the transport kinetics and evaluating the limiting current density in real-time to avoid generating dendritic lithium that can easily penetrate even solid electrolytes.

EXPERIMENTAL PROCEDURES

Materials

The battery grade electrolyte (1 M $LiPF_6$ in ethylene carbonate/dimethyl carbonate with a volume ratio of 1:1), and Whatman AAO membranes (100 and 200 nm pore diameter, 60 μm thickness, 13 mm disk diameter) were purchased from Sigma-Aldrich and used as received. Copper wires, stainless steel wires, 127-μm-thick PVDF, 50-μm-thick PTFE sheets were purchased from McMaster-Carr. The 5-μL glass

capillaries were purchased from VWR. Lithium chips (99.9% purity, 250 and 450 μm thickness, 15.6 mm diameter), and ceramic-coated PE battery separator (2-μm-thick layer of Al_2O_3 particles on both sides of the 12-μm-thick PE separator) were purchased from MTI.

Sandwich Cell

The split test cells (MTI) were used to construct the sandwich cells, following the procedures in a previous report.[10] The sandwich structure consists of two stainless steel (SS) current collectors, two identical lithium chips, two washers punched out of the 127-μm-thick PVDF sheet with an inner diameter of 8 mm, and a single AAO membrane. During the assembling process, excess electrolyte was dispensed to ensure the compartment created by the washer, between Li and AAO, is fully filled, and AAO completely wetted. The stack of SS|Li|Washer|AAO|Washer|Li|SS was sealed in the split cell. The sandwich cells were used to investigate the interaction between lithium growths and the separator at various applied current densities. By placing the electrolyte-filled compartments between lithium electrode and the brittle AAO, we were able to infer whether lithium penetrates the AAO or is blocked by the nanoporous membrane, thus filling the electrolyte compartment before mechanical failure (i.e., AAO cracks due to the pressure applied by the growing lithium deposit). For the sandwich cells using the ceramic-coated PE separator, only one washer punched out of the 50-μm-thick PTFE sheet with an inner diameter of 8 mm was used between the separator and the lithium working electrode to define the active electrode area. The stack sealed in the split cell was SS|Li|Separator|Washer|Li|SS instead.

Junction Cell

A 3-cm segment was first cut from a VWR glass capillary. Two such capillaries were then aligned and fixed onto a glass slide by adhesive tape. A small piece of the AAO (1–2 mm^2) was then inserted between the capillaries. A drop of epoxy was dispensed to seal the junction and allowed to cure overnight. The empty cells were transferred into an argon-filled glovebox (Vigor Gloveboxes). The electrolyte was introduced into the cell via capillary action starting on one side of the cell, wetting the AAO, and then filling the other side of the cell. Thin filaments of lithium were cut from the lithium chip and pushed into either capillary by a stainless steel wire to form a symmetric cell.

Measurement and Characterization

All measurements were performed at room temperature in an argon-filled glovebox with the water and the oxygen concentrations less than 1 ppm. Electrochemical responses of the junction cells as well as the sandwich cells were collected using the Arbin battery testers (BT, 2043 and LBT, 20084, Arbin Instruments). Operando snapshots were captured by an optical microscope (MU500, AmScope). SEM images were obtained with the analytical electron microscopes (JEOL 6010L at MIT, JEOL 7001LFV and FEI Nova NanoSEM 230 at Washington University in St. Louis).

ACKNOWLEDGMENTS

This work was supported by a grant from Robert Bosch LLC through the MIT Energy Initiative (MITei). The experiments using commercial ceramic-coated polyethylene separator were partially supported by IMSE (Institute of Materials Science and Engineering) and by a grant from InCEES (International Center for Energy, Environment and Sustainability) at Washington University in Saint Louis. P.B. acknowledges the startup support from Washington University in St. Louis. J.L. acknowledges support by NSF DMR-1410636. M.Z.B. acknowledges partial support from the Global

Climate and Energy Project at Stanford University and by the US Department of Energy, Basic Energy Sciences through the SUNCAT Center for Interface Science and Catalysis.

AUTHOR CONTRIBUTIONS

Conceptualization, P.B. and M.Z.B.; Methodology, P.B.; Investigation, P.B., J.G., and M.W.; Writing – Original Draft, P.B.; Writing – Review & Editing, P.B., M.W., A.K., J.L., F.R.B., and M.Z.B.; Funding Acquisition, P.B., F.R.B., and M.Z.B.; Resources, L.S.; Supervision, P.B., F.R.B., and M.Z.B.

DECLARATION OF INTERESTS

The authors declare no competing interests.

Received: April 13, 2018
Revised: July 25, 2018
Accepted: August 30, 2018
Published: September 20, 2018

REFERENCES

1. Manthiram, A., Yu, X., and Wang, S. (2017). Lithium battery chemistries enabled by solid-state electrolytes. Nat. Rev. Mater. *2*, 16103.

2. Xu, W., Wang, J., Ding, F., Chen, X., Nasybutin, E., Zhang, Y., and Zhang, J.-G. (2014). Lithium metal anodes for rechargeable batteries. Energ Environ. Sci. *7*, 513–537.

3. Choi, J.W., and Aurbach, D. (2016). Promise and reality of post-lithium-ion batteries with high energy densities. Nat. Rev. Mater. *1*, 16013.

4. Christensen, J., Albertus, P., Sanchez-Carrera, R.S., Lohmann, T., Kozinsky, B., Liedtke, R., Ahmed, J., and Kojic, A. (2012). A critical review of Li/Air batteries. J. Electrochem. Soc. *159*, R1–R30.

5. Albertus, P., Babinec, S., Litzelman, S., and Newman, A. (2018). Status and challenges in enabling the lithium metal electrode for high-energy and low-cost rechargeable batteries. Nat. Energy *3*, 16–21.

6. Lv, D.P., Shao, Y.Y., Lozano, T., Bennett, W.D., Graff, G.L., Polzin, B., Zhang, J.G., Engelhard, M.H., Saenz, N.T., Henderson, W.A., et al. (2015). Failure mechanism for fast-charged lithium metal batteries with liquid electrolytes. Adv. Energy Mater. *5*, https://doi.org/10.1002/aenm.201400993.

7. Aurbach, D., Zinigrad, E., Cohen, Y., and Teller, H. (2002). A short review of failure mechanisms of lithium metal and lithiated graphite anodes in liquid electrolyte solutions. Solid State Ionics *148*, 405–416.

8. Aurbach, D., Zinigrad, E., Teller, H., and Dan, P. (2000). Factors which limit the cycle life of rechargeable lithium (metal) batteries. J. Electrochem. Soc. *147*, 1274–1279.

9. Jiao, S., Zheng, J., Li, Q., Li, X., Engelhard, M.H., Cao, R., Zhang, J.-G., and Xu, W. (2018). Behavior of lithium metal anodes under various capacity utilization and high current density in lithium metal batteries. Joule *2*, 110–124.

10. Bai, P., Li, J., Brushett, F.R., and Bazant, M.Z. (2016). Transition of lithium growth mechanisms in liquid electrolytes. Energ Environ. Sci. *9*, 3221–3229.

11. Yamaki, J., Tobishima, S., Hayashi, K., Saito, K., Nemoto, Y., and Arakawa, M. (1998). A consideration of the morphology of electrochemically deposited lithium in an organic electrolyte. J Power Sources *74*, 219–227.

12. Zheng, G.Y., Lee, S.W., Liang, Z., Lee, H.W., Yan, K., Yao, H., Wang, H., Li, W., Chu, S., and Cui, Y. (2014). Interconnected hollow carbon nanospheres for stable lithium metal anodes. Nat. Nanotechnol. *9*, 618–623.

13. Qian, J.F., Henderson, W.A., Xu, W., Bhattacharya, P., Engelhard, M., Borodin, O., and Zhang, J.G. (2015). High rate and stable cycling of lithium metal anode. Nat. Commun. *6*, 6362.

14. Miao, R.R., Yang, J., Xu, Z.X., Wang, J.L., Nuli, Y., and Sun, L.M. (2016). A new ether-based electrolyte for dendrite-free lithium-metal based rechargeable batteries. Sci. Rep. *6*, 21771.

15. Peled, E., and Menkin, S. (2017). Review—SEI: past, present and future. J. Electrochem. Soc. *164*, A1703–A1719.

16. Peled, E., Golodnitsky, D., and Ardel, G. (1997). Advanced model for solid electrolyte interphase electrodes in liquid and polymer electrolytes. J. Electrochem. Soc. *144*, L208–L210.

17. Peled, E. (1979). The electrochemical behavior of alkali and alkaline earth metals in nonaqueous battery systems—the solid electrolyte interphase model. J. Electrochem. Soc. *126*, 2047–2051.

18. Odziemkowski, M., and Irish, D.E. (1992). An electrochemical study of the reactivity at the lithium electrolyte/bare lithium metal interface: I. purified electrolytes. J. Electrochem. Soc. *139*, 3063–3074.

19. Kushima, A., So, K.P., Su, C., Bai, P., Kuriyama, N., Maebashi, T., Fujiwara, Y., Bazant, M.Z., and Li, J. (2017). Liquid cell transmission electron microscopy observation of lithium metal growth and dissolution: root growth, dead lithium and lithium flotsams. Nano Energy *32*, 271–279.

20. Pinson, M.B., and Bazant, M.Z. (2013). Theory of SEI formation in rechargeable batteries: capacity fade, accelerated aging and lifetime prediction. J. Electrochem. Soc. *160*, A243–A250.

21. Ely, D.R., Jana, A., and García, R.E. (2014). Phase field kinetics of lithium electrodeposits. J. Power Sources *272*, 581–594.

22. Jana, A., Ely, D.R., and García, R.E. (2015). Dendrite-separator interactions in lithium-based batteries. J. Power Sources *275*, 912–921.

23. Winter, M. (2009). The solid electrolyte interphase – the most important and the least understood solid electrolyte in rechargeable Li batteries. Z. Phys. Chem. *223*, 1395–1406.

24. Wu, B., Lochala, J., Taverne, T., and Xiao, J. (2017). The interplay between solid electrolyte interface (SEI) and dendritic lithium growth. Nano Energy *40*, 34–41.

25. Jana, A., and García, R.E. (2017). Lithium dendrite growth mechanisms in liquid electrolytes. Nano Energy *41*, 552–565.

26. Zhengyuan, T., Yu, K., Yingying, L., and Archer, A.L. (2014). Nanoporous polymer-ceramic composite electrolytes for lithium metal batteries. Adv. Energy Mater. *4*, 1300654.

27. Zhengyuan, T., Yingying, L., and Lynden, A. (2015). A dendrite-free lithium metal battery model based on nanoporous polymer/ceramic composite electrolytes and high-energy electrodes. Small *11*, 2631–2635.

28. Finegan, D.P., Cooper, S.J., Tjaden, B., Taiwo, O.O., Gelb, J., Hinds, G., Brett, D.J.L., and Shearing, P.R. (2016). Characterising the structural properties of polymer separators for lithium-ion batteries in 3D using phase contrast X-ray microscopy. J. Power Sources *333*, 184–192.

29. Ferguson, T.R., and Bazant, M.Z. (2012). Nonequilibrium thermodynamics of porous electrodes. J. Electrochem. Soc. *159*, A1967–A1985.

30. Kerman, K., Luntz, A., Viswanathan, V., Chiang, Y.-M., and Chen, Z. (2017). Review—practical challenges hindering the development of solid state Li ion batteries. J. Electrochem. Soc. *164*, A1731–A1744.

31. Sharafi, A., Meyer, H.M., Nanda, J., Wolfenstine, J., and Sakamoto, J. (2016). Characterizing the Li-Li7La3Zr2O12 interface stability and kinetics as a function of temperature and current density. J. Power Sources *302*, 135–139.

32. Basappa, R.H., Ito, T., and Yamada, H. (2017). Contact between garnet-type solid electrolyte and lithium metal anode: influence on charge transfer resistance and short circuit prevention. J. Electrochem. Soc. *164*, A666–A671.

33. Ishiguro, K., Nakata, Y., Matsui, M., Uechi, I., Takeda, Y., Yamamoto, O., and Imanishi, N. (2013). Stability of Nb-doped cubic Li7La3Zr2O12 with lithium metal. J. Electrochem. Soc. *160*, A1690–A1693.

34. Ren, Y., Shen, Y., Lin, Y., and Nan, C.-W. (2015). Direct observation of lithium dendrites inside garnet-type lithium-ion solid electrolyte. Electrochem. Commun. *57*, 27–30.

35. Tikekar, M.D., Archer, L.A., and Koch, D.L. (2016). Stabilizing electrodeposition in elastic solid electrolytes containing immobilized anions. Sci. Adv. *2*, e1600320.

36. Tikekar, M.D., Archer, L.A., and Koch, D.L. (2014). Stability analysis of electrodeposition across a structured electrolyte with immobilized anions. J. Electrochem. Soc. *161*, A847–A855.

37. Monroe, C., and Newman, J. (2005). The impact of elastic deformation on deposition kinetics at lithium/polymer interfaces. J. Electrochem. Soc. *152*, A396–A404.

38. Barai, P., Higa, K., and Srinivasan, V. (2017). Effect of initial state of lithium on the propensity for dendrite formation: a theoretical study. J. Electrochem. Soc. *164*, A180–A189.

39. Barai, P., Higa, K., and Srinivasan, V. (2017). Lithium dendrite growth mechanisms in polymer electrolytes and prevention strategies. Phys. Chem. Chem. Phys. *19*, 20493–20505.

40. Porz, L., Swamy, T., Sheldon, B.W., Rettenwander, D., Frömling, T., Thaman, H.L., Berendts, S., Uecker, R., Carter, W.C., and Chiang, Y.-M. (2017). Mechanism of lithium metal penetration through inorganic solid electrolytes. Adv. Energy Mater. *7*, 1701003.

41. Wu, B., Wang, S., Lochala, J., Desrochers, D., Liu, B., Zhang, W., Yang, J., and Xiao, J. (2018). The role of the solid electrolyte interphase layer in preventing Li dendrite growth in solid-state batteries. Energy Environ. Sci. *11*, 1803–1810.

42. Wood, K.N., Noked, M., and Dasgupta, N.P. (2017). Lithium metal anodes: toward an improved understanding of coupled morphological, electrochemical, and mechanical behavior. ACS Energy Lett. *2*, 664–672.